ChemCatChem

Research Article
doi.org/10.1002/cctc.202500233

Chemistry Europe
European Chemical Societies Publishing

www.chemcatchem.org

Polyolefin and Polystyrene-Derived Carbon Nanotubes: Catalysts for Oxidative Desulfurization Under a Biphasic System

Fernanda F. Roman,*[a, b, c] Maria C. Batista,[a, d] Adriano S. Silva,[a, b, c] Ana Júlia Briganti Bezerra,[a] Jose L. de Diaz de Tuesta,[e, f] Raquel V. Mambrini,[d] Adrián M. T. Silva,[b, c] Joaquim L. Faria,[b, c] and Helder T. Gomes*[a]

The conversion of plastic solid waste into carbon nanotubes (CNTs) via chemical vapor deposition (CVD) and the effectiveness of these CNTs as catalysts for oxidative desulfurization (ODS) of a simulated fuel were investigated. The primary focus is on the use of CNTs synthesized from various polymer sources, including polyolefins and polystyrene (PS), to remove sulfur compounds using hydrogen peroxide (H_2O_2) as an oxidant. The surface modification of CNTs by using acids (H_2SO_4 or HNO_3), the influence of the carbon feedstock (polyolefins vs PS), the use of co-catalysts, and the effect of the extractant phase were all evaluated on the oxidative removal of dibenzothiophene from a simulated fuel. Results revealed that CNTs derived from polyolefins displayed higher desulfurization efficiency (up to 77% in 8 h), with nitric acid-treated CNTs showing the best performance under oil-water biphasic systems. Replacing water with acetonitrile and adding a co-catalyst (formic acid) resulted in a desulfurization of 91% in 2 h of reaction. Under certain conditions, C—S bond cleavage was observed. This research contributes to the valorization of plastic solid waste and the reduction of atmospheric pollution, promoting circular economy practices and environmental sustainability.

1. Introduction

Despite advancements in renewable energy sources, recent data from the Statistical Review of World Energy, 2023 reveal a notable increase in oil consumption, amounting to 9.8 million barrels per day in 2022.[1] Although the composition of crude oil varies based on its location, the fundamental composition remains relatively consistent.[2] Among its constituents, sulfur-containing compounds can be highlighted, as they are the most abundant heteroatom in crude oil, ranging from 0.06 to 8 wt.%.[2] The combustion of fuels containing sulfur-based compounds has grave consequences for health and the environment,[3] which have resulted in increased restrictions on its presence in fuels. Currently, the EU allows 10 ppm of S for both diesel and gasoline, and many other countries adopt similar limits or are on the path toward limiting S concentration to similar levels.[4] The expected tendency is to reach sulfur-free fuels at some point.

Hydrodesulfurization (HDS) is currently used at the industrial level for desulfurization purposes, usually operating at around 300 °C and 5–50 bar of H_2 partial pressure.[2,4] However, some sulfur-containing compounds, such as those containing a thiophene ring, are refractory to typical HDS conditions and may require higher temperature and pressure (up to 425 °C and 170 bar).[2] Alternatives, such as oxidative desulfurization (ODS) have been seen as a suitable complement to achieving the low levels of S, or possibly sulfur-free, fuels required by the law.[2]

ODS is a process where sulfur-containing molecules are oxidized, usually into sulfoxides and sulfones, which can be subsequently extracted.[5] This method is promising because it can be conducted at mild temperatures (<100 °C), under atmospheric pressure, and does not require hydrogen.[6] Various oxidizing agents have been explored (gaseous, such as O_2, air, ozone, and NO_2,[7] and organic hydroperoxides, such as tert-butyl hydroperoxide and cumene hydroperoxide[8]), with hydrogen peroxide (H_2O_2) being largely used for ODS purposes due to its environmental friendliness, commercial availability, and high oxidative ability.[9,10] However, H_2O_2 promotes the formation of a

[a] F. F. Roman, M. C. Batista, A. S. Silva, A. J. B. Bezerra, Prof. Dr. H. T. Gomes
CIMO, LA SusTEC, Instituto Politécnico de Bragança, Alameda de Santa Apolónia, s/n, Bragança 5300-253, Portugal
E-mail: roman@ipb.pt
htgomes@ipb.pt

[b] F. F. Roman, A. S. Silva, Prof. Dr. A. M. T. Silva, Prof. Dr. J. L. Faria
LSRE-LCM, Laboratory of Separation and Reaction Engineering, Laboratory of Catalysis and Materials, Faculty of Engineering, University of Porto, Rua Dr. Roberto Frias, Porto 4200-465, Portugal

[c] F. F. Roman, A. S. Silva, Prof. Dr. A. M. T. Silva, Prof. Dr. J. L. Faria
ALiCE, Associate Laboratory in Chemical Engineering, Rua Dr. Roberto Frias, Porto 4200-465, Portugal

[d] M. C. Batista, Prof. Dr. R. V. Mambrini
Departamento de Química, Centro Federal de Educação Tecnológica de Minas Gerais (CEFET-MG), Campus I, Belo Horizonte 30421–169, Brazil

[e] Dr. J. L. de Diaz de Tuesta
Chemical and Environmental Engineering Group, ESCET, Universidad Rey Juan Carlos, Tulipán s/n, Móstoles 28933, Spain

[f] Dr. J. L. de Diaz de Tuesta
Instituto de Investigación de Tecnologías para la Sostenibilidad, Universidad Rey Juan Carlos, C/Tulipán s/n, Móstoles 28933, Spain

Supporting information for this article is available on the WWW under https://doi.org/10.1002/cctc.202500233

two-phase system. To address this issue, catalysts are employed to facilitate the decomposition of H_2O_2 and enhance the interaction between phases.[11]

Typical catalysts for desulfurization purposes are based on metal oxides and polyoxometalates, usually containing metal active centers such as tungsten, molybdenum, vanadium, palladium, among others.[12] However, most ODS catalysts can be unsustainable due to metal scarcity[13] or metal extraction.[14] A suitable way to increase the sustainability of ODS systems is to use catalysts obtained from renewable or waste resources.[2] In this sense, carbon nanotubes (CNTs) can be interesting alternatives because they can be synthesized from any carbon-rich precursor,[15] including plastic solid waste. Replacing typical non-renewable carbon sources (such as methane and ethylene) in CNTs synthesis by wastes has been shown to significantly reduce the impacts of CNTs production, including reduction of CO_2 emissions[16,17] and a decrease in the depletion of fossil resources and human toxicity.[16] Furthermore, CNTs have been shown to catalyze the decomposition of H_2O_2 into highly oxidizing hydroxyl radicals in both monophasic[18,19] and biphasic systems.[20,21] The extractant phase also plays a vital role in ODS. Most commonly, acetonitrile is used as extractant; however, aqueous phases could present advantages such as lower environmental impact (such as reduced toxicity and emissions compared to organic solvents)[22,23] and easier phase separation[24] (facilitating oil recovery after ODS), making them more sustainable alternatives.[25]

This research is centered on the development and assessment of a range of CNTs derived from polymeric materials, simulating plastic solid waste. The CNTs were then tested as catalysts for the biphasic ODS, aiming at degrading a model contaminant, dibenzothiophene (DBT) in 2,2,4-trimethylpentane, simulating a contaminated fuel. H_2O_2 was chosen as the oxidant source, and two extractant phases were compared: water and acetonitrile. Furthermore, the use of co-catalysts (formic acid and sulfuric acid) was also evaluated.

2. Results and Discussion

2.1. Materials Synthesis and Characterization

2.1.1. Catalyst for Chemical Vapor Deposition (CVD)

The X-ray diffraction (XRD) of the CVD catalyst used to grow the CNT structures ($NiFe/Al_2O_3$) is shown in Figure S1a. The results were analyzed with the aid of the software X'Pert HighScore Plus (v4.5) loaded with Crystallography Open Database (COD) cards. The qualitative analysis revealed that the sample contains alumina, both gamma (γ-) and alpha (α-) phases (COD card 96-152-8248 and 96-201-5531, respectively, Figure S2), with semi-quantitative analysis estimated as 54% and 28%, respectively (representing a total of 82% of the CVD catalyst). Three different metal phases were identified in the X-ray diffractograms: nickel ferrite spinel, hematite and nickel oxide, according to COD cards 96-100-6116, 96-900-9783, and 96-101-0094, respectively. Each phase was estimated to correspond to 6% of the CVD catalyst, amounting to a total of 18% of active phase. Crystallite sizes were estimated using Halder-Wagner and size strain plot. Hematite was estimated at 7.26 and 9.76 nm, respectively, nickel ferrite at 7.32 and 11.95 nm, respectively, and nickel oxide at 7.35 and 9.63 nm, respectively. The content of Ni and Fe (Table 1), as determined by atomic absorption, was estimated at 4.9 and 8.8 wt.%, respectively. The Fourier-transform infrared spectroscopy (FTIR) spectrum is displayed in Figure S1b. Bands related to adsorbed water were identified (-OH stretching vibration at 1636 and 1384 cm^{-1}[26]). The band located around 620 cm^{-1} can be attributed to the intrinsic stretching of $NiFe_2O_4$ at the tetrahedral vibration site[27] or from Ni-O bands from nickel oxide particles.[26] The band at 820 cm^{-1} was ascribed to Al-O stretch from alumina[28] and the band at 738 cm^{-1} was ascribed to the Al-O-Al stretching vibration.[29] The broadband in the region 400-1000 cm^{-1} is also a characteristic of amorphous and disordered γ-alumina,[30] which was identified in most abundance by XRD.

2.1.2. Carbon Nanotubes

Different samples of CNTs were prepared: **CNT-POL** refers to a sample obtained with a mixture of the three polyolefins (LDPE, HDPE, and PP in 35:25:40 mass ratio); **CNT-PS** is derived from PS; **CNT-MIX** results from a mixture of the four polymers (LDPE, HDPE, PP, and PS in 31:23:35:11 mass ratio); these three samples were subjected to strong oxidation with nitric acid (69 wt.% HNO_3, 130 °C, 24 h) to introduce oxygenated moieties (**CNT-POL-OX**, **CNT-PS-OX**, and **CNT-MIX-OX**, respectively); and **CNT-POL-P** corresponds to CNT-POL subjected to a sulfuric acid wash (50 wt.% H_2SO_4, 140 °C, 3 h).

The yield of CNT samples (as calculated by Equation 1 – Experimental Section) is displayed in Figure S3. As seen, the overall yield is very similar (25%–30%) for all three non-oxidized samples of CNTs, with a slight improvement in the yield for the single polymer (CNT-PS) compared to the polymer mixtures (CNT-POL and CNT-MIX). Similar yields for CNTs derived from polymers over NiFe-based catalysts have been reported.[31,32] Moreover, when different acids were used to treat the same sample (CNT-POL), the mass loss associated with the acid treatment varied according to the acid used, with HNO_3 resulting in a higher mass loss (47% for CNT-POL-OX) compared to H_2SO_4 (42% for CNT-POL-P). Given the distinct conditions (acid concentration and time of exposure) used for HNO_3 treatment, this result was expected.

Transmission electron microscopy (TEM) images of the CNTs are displayed in Figure 1. CNT-POL-P (Figure 1a–c) and CNT-POL-OX (Figure 1d–f) samples consist of filamentous structures with mostly straight walls. The average outer diameter for CNT-POL-P and CNT-POL-OX was estimated at 28.2 ± 0.6 nm and 22.8 ± 0.6 nm, respectively (Figure S4a,b). CNT-MIX-OX resulted in some structures with straight walls, but it is also possible to see some CNTs with more disordered walls (Figure 1j–l), with an average outer diameter of 23.8 ± 3 nm (Figure S4c). Finally, CNT-PS-OX resulted in more disordered CNTs, with some growing with a cup-stacked structure (Figure 1i) and including some coiled CNT bundles (Figure 1g,h), and an average diameter of 17.5 ± 0.7 nm (Figure S4d). Other works also reported that PS

Table 1. Elemental analysis, Ni and Fe contents, textural properties, and surface chemistry.

Material	C [%]	H [%]	N [%]	Ni [%]	Fe [%]	O [%]	S_{BET} [m^2 g^{-1}]	Total Pore Volume [mm^3 g^{-1}]	Acidity [μmol g^{-1}]	Basicity [μmol g^{-1}]	CA [°]	Image
CNT-POL	59.2± 2.8	0.18± 0.02	–	2.6± 0.05	4.3± 0.1	2.6± 0.3[a)]	144	575	1551	138	138 ± 2°	
CNT-POL-P	97.4± 0.9	0.04± <0.01	–	0.5± 0.01	1.1± 0.1	1.0± 0.1[a)]	148	359	982	25	126 ± 2°	
CNT-POL-OX	90.9± 0.3	0.15± 0.01	0.11± <0.01	0.3± <0.01	0.7± 0.1	4.4± 0.1[a)]	214	632	1695	368	117 ± 3°	
CNT-PS-OX	87.7± 0.2	0.28± 0.10	0.16± 0.01	<0.01	0.1± 0.06	10.7[b)]	226	794	1897	465	51 ± 5°	
CNT-MIX-OX	89.6± 1.7	0.24± 0.01	0.12± <0.01	0.04± <0.01	0.3± 0.01	9.6[b)]	219	592	1758	342	101 ± 4°	
NiFe/Al_2O_3	–	–	–	8.8± <0.01	4.9± <0.01	–	134	427	1840	796	105 ± 5°	
Al_2O_3	–	–	–	–	–	–	221	508	1836	1270	22 ± 4°	

[a)] obtained from elemental analysis;
[b)] obtained from difference 100-ashes-C-H-N-S. CA = water contact angle.

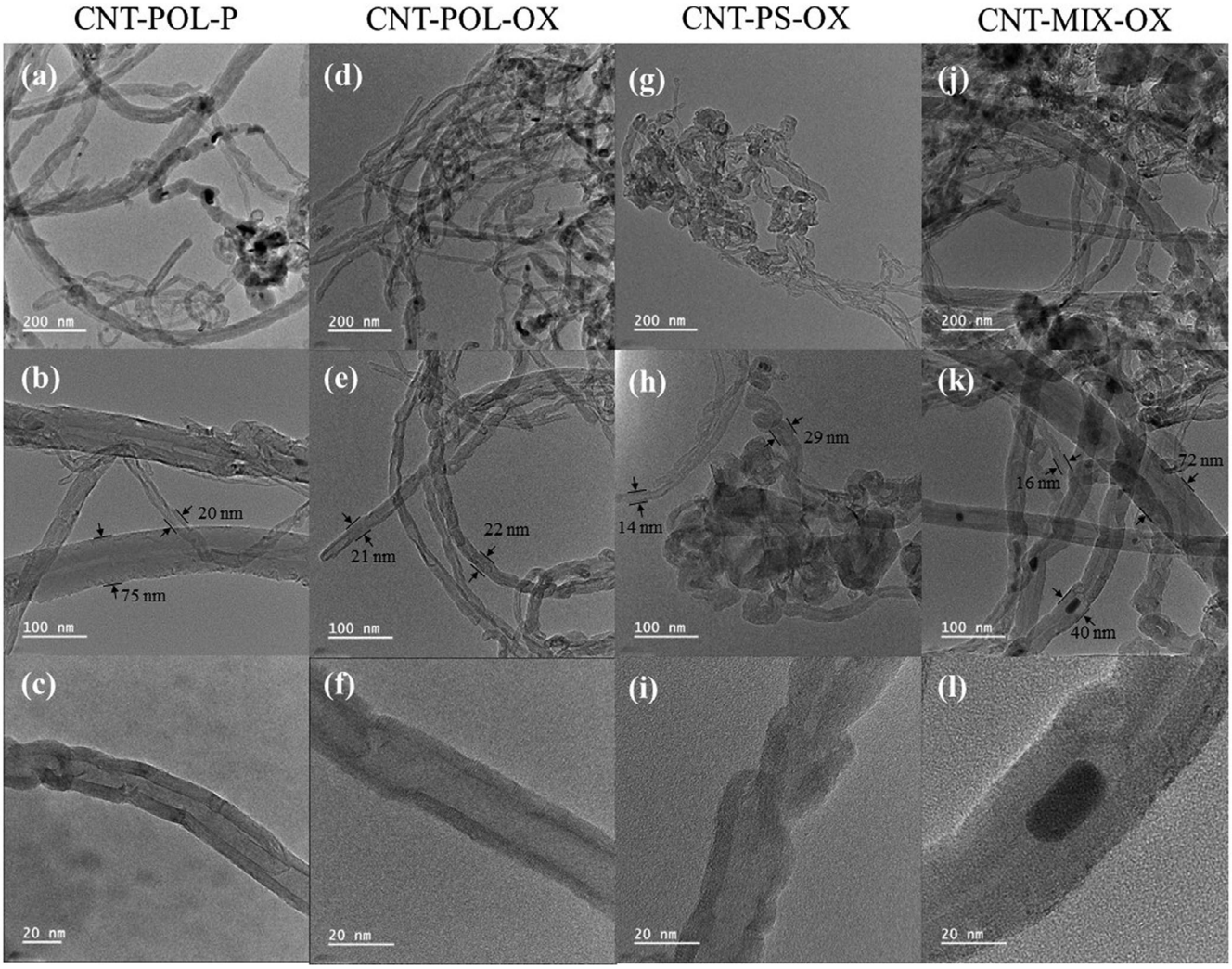

Figure 1. TEM images of (a–c) CNT-POL-P, (d–f) CNT-POL-OX, (g–i) CNT-PS-OX, and (j–l) CNT-MIX-OX.

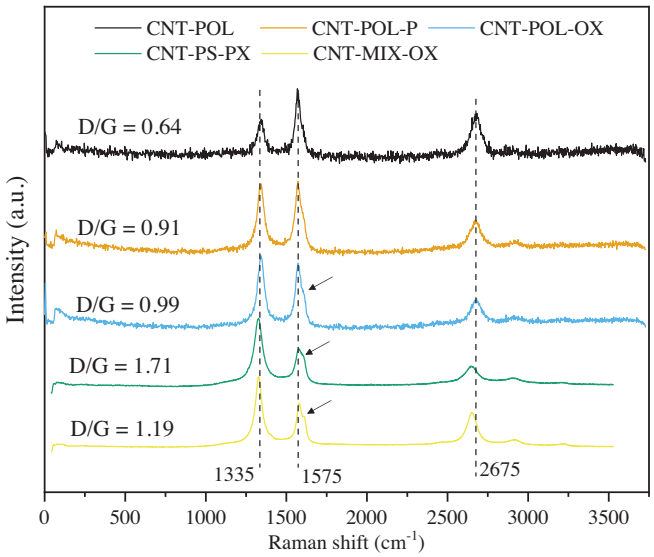

Figure 2. Raman spectra of the CNTs.

yields CNTs with more irregular and defective CNTs compared to polyolefins.[33] Similar outer diameters have been reported for CNTs derived from polyolefins (either as mixtures[15,34] or single polymers[18,35]) and polystyrene.[36]

The Raman spectra of the CNTs are displayed in Figure 2. There are three clear bands: the G-band around 1575 cm^{-1}, ascribed to the graphitic form of CNTs, the D-band around 1335 cm^{-1}, ascribed to defects in the carbon phase, and the G′-band around 2675 cm^{-1}, also ascribed to graphitic carbon phases. In the materials oxidized with HNO_3, a fourth band is also observed, located near ca. 1620 cm^{-1}(indicated with an arrow in Figure 2), known as the D′-band, and typically associated with defects in the structure of the material.[37] For the originally synthesized CNT-POL, the G-band is obviously more intense than the D-band, indicating a more graphitic material, and translating into a D/G ratio of 0.64. The acid treatment increases the disorder of the materials due to the introduction of surface groups or destruction of graphitic layers,[38] and it seems that stronger oxidizing conditions result in more defects in the structure, as shown for CNT-POL-P and CNT-POL-OX (D/G ratios of 0.91 and 0.99, respectively). Nevertheless, the choice of the polymer precursor has a higher impact on the graphitization of the material, as CNT-MIX-OX and CNT-PS-OX both resulted in an increased D/G ratio (1.19 and 1.71, respectively) compared to CNT-POL-OX (0.99). A correlation between the percentual of PS in the polymer precursor and the D/G ratio of oxidized samples seems to exist (Figure S5). Previous works also reported higher defects for PS-derived CNTs[33] compared to polyolefins-derived materials.

The elemental content (C, H, N, S, O, Ni, and Fe) and ashes in the different materials are displayed in Table 1. The content of C in all acid-treated CNTs is above ca. 90%, whereas for the original CNT-POL, it represents around 59% of the material, due to the high content of ashes (48%). CNT-POL-P resulted in the highest content of C (97%), likely due to the low incorporation of other atoms (S, H, N, and O are below 1%) allied to a high removal of the ash content (ca. 1.5%). Acid-treated samples resulted in low ash content (<5%). N-content arises from HNO_3 attack and is moreover the same for the CNTs (0.11%–0.16%) with more defective materials, resulting in a slightly higher content of N; S was only identified in CNT-POL-P (0.11% ± 0.01%). The content of oxygen in the carbon nanotube structure varied significantly according to both acid treatment and polymer source. PS-containing materials (CNT-PS-OX and CNT-MIX-OX) resulted in more significant incorporation of oxygen (9.6%–10.7%), compared to CNT-POL-OX (4.4%), and HNO_3 treatment also allowed more oxygen into the material compared to H_2SO_4 (1.0% for CNT-POL-P). The content of oxygen in CNT-POL likely arises from oxygen transfer from the metallic particle during its reduction in a carbon-rich atmosphere, as shown elsewhere.[39] Ni and Fe represent very little content for all acid-treated materials (<1.1%), indicating successful removal of the metallic particles during acid washing. It should be noted that the ash content estimated for CNT-POL does not seem correct at first glance (considering that the sum of ashes and C content surpasses 100%). We attribute this fact to the partial or complete oxidation of metallic particles during thermogravimetric analysis (TGA) analysis (in which ash content was estimated). It is well-established that during CVD reaction, a reduction of metallic phases can occur due to the reducing atmosphere from the hydrogen gas generated during CNT growth. In fact, in previous works of our group, we have reported that after the CVD reaction, the main phase for Fe is cementite.[18] Other works have also reported the identification of cementite and zero-valent iron[40] as a result of the CVD reaction. These reduced iron phases can be easily oxidized during TGA.[18] Previous works have reported an average mass increase of 132% for Fe^0 starting at 450°C up to 585 °C,[41] and 125%–130% for Ni^0 in the temperature range of 25–900 °C.[42]

Figure 3 shows TGA and derivative thermogravimetry (DTG) profiles for the CNTs. CNT-PS-OX and CNT-MIX-OX start to decompose at lower temperatures (ca. 250–300 °C) compared to the samples derived from polyolefins (>450 °C), indicating that PS-containing CNTs are less stable toward oxidation compared to POL-derived CNTs. Similarly, the main event of mass loss for PS-derived materials is located at a lower temperature (565–588 °C) compared to polyolefin-derived materials (636–650 °C). This behavior is correlated with the lower-quality CNT obtained with PS as carbon precursor (as previously seen in TEM and Raman analysis). In general, more stable CNTs indicate a higher structural order and a lower number of defects.[43] Mass loss at temperatures below 500 °C is usually associated with amorphous carbon phases,[15] and both PS-containing samples have a mass loss in the range 150–450 °C (representing ca. 10.4% and 6.9%, respectively, for CNT-PS-OX and CNT-MIX-OX). CNT-POL resulted in a slightly lower mass loss center (636 °C) compared to CNT-POL-P and CNT-POL-OX, due to the catalytic effect from the metal particles within the CNTs.[44] Any mass loss below 150 °C is associated with moisture.

The textural properties of the materials are displayed in Table 1, and the adsorption–desorption isotherms are reported in Figure S6. Both the starting polymer and the acid treatment affect the surface area of the materials. For the type of polymer, PS resulted in materials with higher surface areas than pure polyolefins (CNT-PS-OX > CNT-POL-OX ~ CNT-MIX-OX), likely

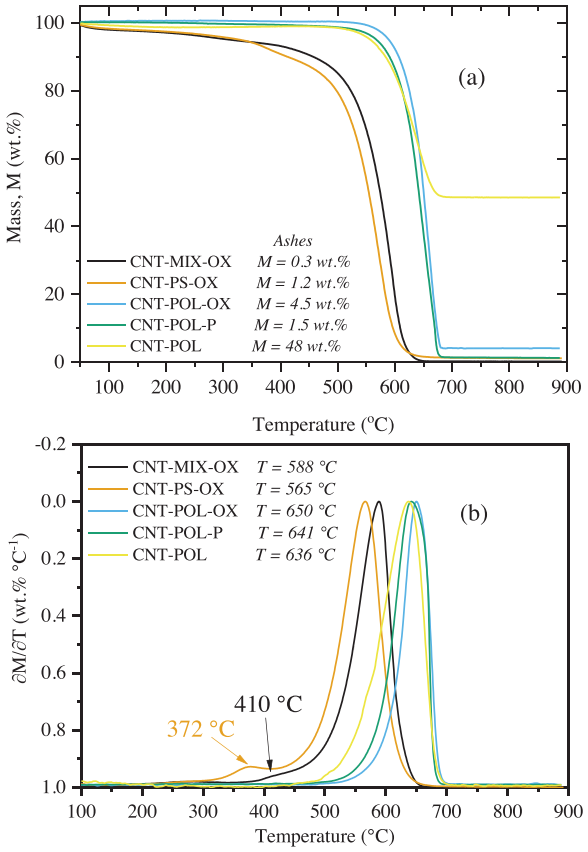

Figure 3. a) TGA and b) DTG of the CNTs. The temperature in (b) is related to the main mass loss event.

associated with the increased number of defects[45] upon PS addition in the feedstock (with a positive correlation with the D/G ratio, Figure S7a). In addition, the type of acid treatment influences the surface area as well, as both acid treatments increased the surface area of CNT-POL, with HNO_3-treated CNT (CNT-POL-OX) representing an increase of 48%, while H_2SO_4 treatment only resulted in an increase of ca. 3% (CNT-POL-P). Similar effects over the BET area for HNO_3 versus H_2SO_4 treatments have been previously reported.[46] The increase in surface area for acid-treated CNTs is linked to the introduction of defects in the walls of the tubes and to the opening of the tips of CNTs.[45] The CVD catalyst ($NiFe/Al_2O_3$) resulted in a surface area (134 $m^2\ g^{-1}$) lower than the surface area for the support (Al_2O_3, 221 $m^2\ g^{-1}$).

The acidic characterization of the materials is displayed in Table 1. All samples display both acidic and basic surface groups. CNT-POL reveals a high content of acidic groups (1551 μmol g^{-1}); however, we largely attribute this result to the acidity displayed by the CVD catalyst ($NiFe/Al_2O_3$, 1840 μmol g^{-1}). Upon acid washing, the CVD catalyst is removed, decreasing the number of acidic and alkali groups at the surface of CNT-POL-P (982 and 25 μmol g^{-1}, respectively). On the other hand, HNO_3-treatment resulted in an increased number of acidic and alkali sites (1695 and 368 μmol g^{-1}, respectively), due to the introduction of functionalities on the CNT surface. CNT-PS-OX and CNT-MIX-OX resulted in a higher content of surface acidic functionalities (1897 and 1758 μmol g^{-1}, respectively), whereas basic functionalities were introduced in similar amounts compared to CNT-POL-OX (465 and 342 μmol g^{-1}, respectively).

The water contact angle of the samples (Table 1) was heavily influenced by the starting polymer, with CNT-PS-OX resulting in the lowest contact angle (51°), followed by CNT-MIX-OX (101°) and CNT-POL-OX (117°). The wettability of a carbon sample is highly influenced by the functional groups attached to its surface, especially oxygen-containing groups.[47] Thus, the lower contact angle found for CNT-PS-OX is in line with previous characterization results. The acid of choice also influenced the contact angle, although this effect was less pronounced than the polymer tested. CNT-POL resulted in a contact angle of 138°, indicating that it is hydrophobic, a typical characteristic of non-functionalized CNTs.[48] Following functionalization, the contact angle dropped to 126° and 117° for H_2SO_4 and HNO_3 treatments, respectively. The contact angle correlates inversely with the degree of graphitization of the CNTs (Figure S7b) and with the addition of PS in the feedstock (Figure S7c): PS is associated with a higher D/G ratio, resulting in materials with a lower contact angle.

2.2. Desulfurization Runs

2.2.1. Effect of Acid-Treatment

The removal of DBT from the simulated fuel phase according to the acid treatment used is shown in Figure 4. The CVD catalyst ($NiFe/Al_2O_3$) was also tested for comparison purposes. All tested materials displayed catalytic activity toward the removal of DBT (>25%) and H_2O_2 conversion (>15%) when compared to the non-catalytic run—N.C. (removal of DBT and H_2O_2 conversion of 8% and 4%, respectively) in 8 h of reaction. CNT-POL-OX displayed a significantly higher catalytic activity toward the removal of DBT (77%) compared to CNT-POL (58%), CNT-POL-P (ca. 30%), and the CVD catalyst (30%) in 8 h of reaction. For comparison purposes, pure extraction effect under the studied conditions falls below 2% (Figure S8).

On the other hand, the materials displayed distinct behavior toward the decomposition of hydrogen, with $NiFe/Al_2O_3$ decomposing over 90% of the oxidant source in just 60 min of reaction, followed by CNT-POL-OX (66%), CNT-POL (25%), and CNT-POL-P (ca. 6%). The decomposition of hydrogen peroxide was found to be correlated to the amount of acidic groups on the surface of CNTs (Figure S9a, $R^2 > 0.98$). The DBT removal, on the other hand, was positively influenced by the amount of basic groups (Figure S9b, $R^2 > 0.91$) and by the oxygen content (Figure S9c, $R^2 > 0.91$), meaning that the high activity of CNT-POL-OX is likely ascribed to its oxygenated and basic content. The positive influence of oxygenated groups on the surface of carbon-based materials for ODS purposes has been previously reported.[49,50] The reason ascribed for that increased activity is related to the electron-withdrawing capacity of the oxygenated groups; it correlates well with the electron donor ability of the S center from DBT, likely increasing the adsorptive interactions between DBT and catalyst.[2] In fact, among the polyolefin-derived CNTs

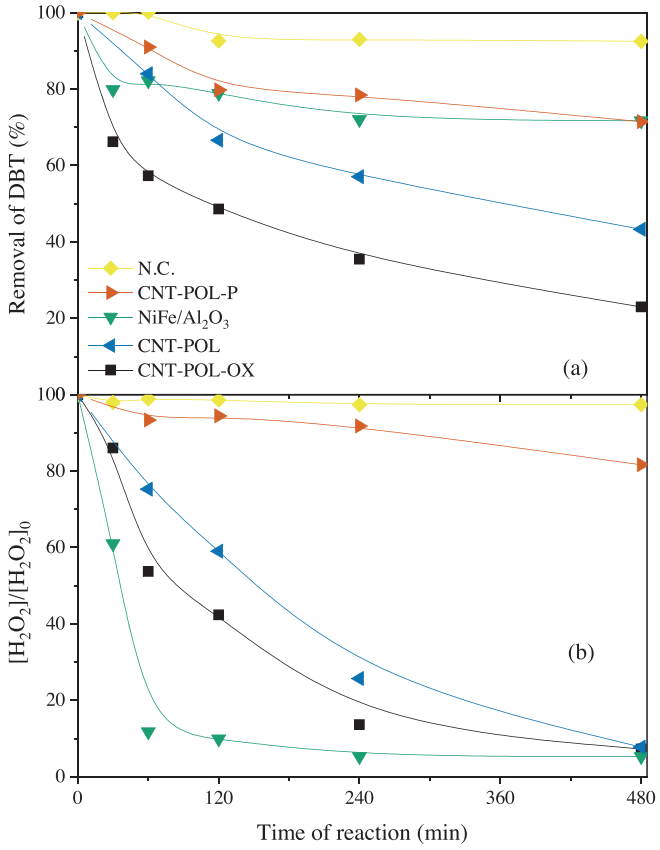

Figure 4. a) Removal of DBT from the oil phase and b) decomposition of H_2O_2 upon time of reaction. Conditions: [DBT]0 = 500 mg L^{-1} in 2,2,4-trimethylpentane, water as extractant phase, O/W volume ration of 80:20, [catalyst] = 2.5 g L^{-1} (considering the whole volume of the system), T = 70 °C, 0.1 vol water.% of 1 M H_2SO_4 (equivalent to a pH_0 of 3.0).

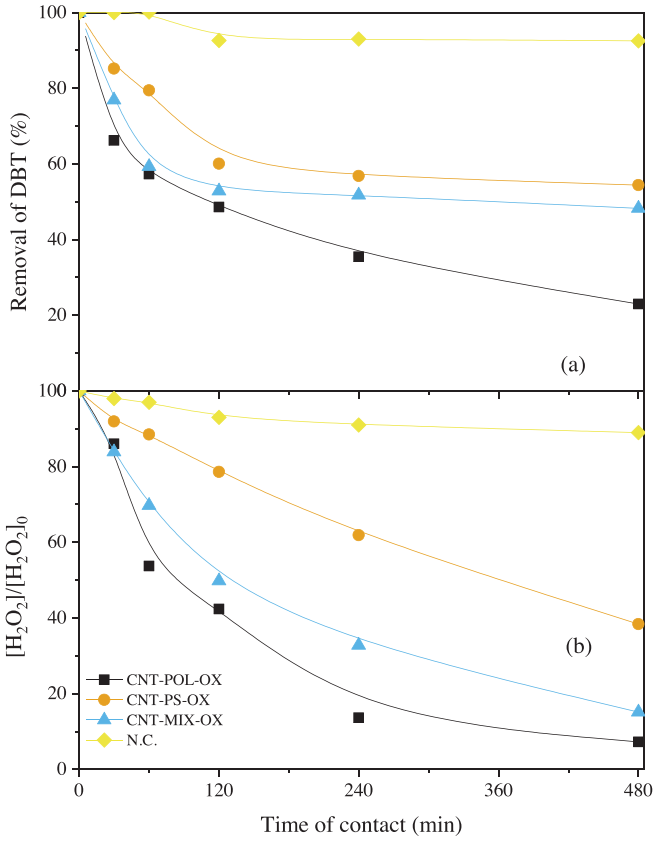

Figure 5. a) Removal of DBT from the oil phase and b) decomposition of H_2O_2 upon time of reaction. Conditions: [DBT]0 = 500 mg L^{-1} in 2,2,4-trimethylpentane, water as extractant phase, O/W volume ration of 80:20, [catalyst] = 2.5 g L^{-1} (considering the whole volume of the system), T = 70 °C, 0.1 volwater.% of 1 M H_2SO_4 (equivalent to a pH_0 of 3.0).

(CNT-POL, CNT-POL-P, and CNT-POL-OX) a positive correlation was found between oxygen content and DBT adsorption (Figure S10b, R^2 = 0.98). CNT-PS-OX resulted in lower DBT adsorption than expected given its oxygen content, although this result may be attributed to its lower contact angle, hindering proper contact with DBT.

By the end of the reaction, the adsorbed products on the catalyst surface were extracted using acetone, and the results regarding the amount of DBT, DBT 5-oxide, and DBT 5,5-dioxide recovered from the CNT surface are reported in Figure S11. As seen, CNT-POL-OX, which revealed a much more efficient ODS reaction, resulted in almost no DBT adsorbed by the end of the reaction; other intermediates (DBT 5-oxide and DBT-5,5-dioxide, Figure S11b) were found in negligible amounts (below 0.1%). Other catalysts resulted in an accumulation of DBT at their surface by the end of the reaction. This accumulation indicates that their primary role, especially CNT-POL-P, was that of an adsorbent rather than a catalyst.

The efficiency of DBT removal (X_{DBT}) per H_2O_2 converted (X_{H2O2}), calculated according to Equation 2–Experimental Section, is shown in Figure S12. As seen, the highest efficiency was achieved in the presence of CNT-POL-P. However, this efficiency was only high because a significant amount of DBT remained adsorbed at the catalyst surface (as shown in Figure S11), allied to a low H_2O_2 decomposition. Given the results reported so far, oxidation of the CNT surface with strong acid (as for CNT-POL-OX) was found more interesting for ODS purposes.

2.2.2. Effect of Carbon Source

The removal of DBT from the simulated fuel phase, when using HNO_3-treated CNTs derived from different polymer feedstocks, is depicted in Figure 5. CNT-POL-OX shows a higher removal rate for DBT than the other two materials (CNT-MIX-OX and CNT-PS-OX), although the differences are not so evident compared to the results obtained in the previous section (Figure 4). CNT-MIX-OX followed a quite similar trend to CNT-POL-OX in the first 2 h of reaction (both with ca. 48%–50% of DBT removal and 55%–58% of H_2O_2 conversion), but the removal of DBT stabilized in ca. 50% up to the end of the experiment. Both CNTs allowed an H_2O_2 decomposition of over 85% in 8 h of reaction. CNT-PS-OX resulted in ca. 42% of DBT removal and 97% of H_2O_2 conversion in 8 h of reaction. The conversion of H_2O_2 was positively correlated to the total volume of pores of the CNTs (Figure S13a, R^2 > 0.94).

As seen in the previous section, the oxygen content was correlated with increased activity toward DBT removal, which all three materials (CNT-POL-OX, CNT-PS-OX, and CNT-MIX-OX) possess. Nevertheless, other parameters may also play

significant roles in biphasic selective oxidation, such as the contact angle (CA). The DBT removal was positively correlated with the CA of the catalyst particles (Figure S13b, $R^2 > 0.89$), especially at the first beginning of the reaction (up to 120 min), with a lower CA resulting in poorer removal of DBT. Other works have also reported that a suitable hydrophobic character is required for desulfurization activity.[51,52] A suitable wettability allows the catalyst particle to properly contact both hydrophobic DBT and hydrophilic H_2O_2. The materials CNT-POL-OX and CNT-MIX-OX both resulted in materials with a better balance between hydrophilic and hydrophobic characteristics (translating into a CA in the range of 100–117°), which explains their similar behavior toward the removal of DBT at the beginning of the reaction. The amount of defects at the material surface, translated into the D/G ratio, was found to inversely correlate to the removal of DBT (Figure S13c, $R^2 > 0.91$), meaning that a higher degree of graphitization favors DBT removal (which also correlates inversely with the CA, as previously shown in Figure S7b). Thus, CNT-POL-OX higher activity toward DBT removal is ascribed to its oxygen and basic content, associated with its suitable wettability (translated into a CA of ca. 117°) and degree of graphitization (D/G ratio).

CNT-MIX-OX resulted in a higher content of DBT remaining adsorbed at its surface by the end of the reaction (Figure S11). Other sulfonated compounds (DBT 5-oxide and DBT 5,5-dioxide) were also found upon extraction from the catalyst, representing less than 0.5% of the initially loaded S content for both CNT-PS-OX and CNT-MIX-OX.

2.2.3. Effect of Extractant and Acid Addition

Considering the higher catalytic activity of CNT-POL-OX (Figure 5), experiments were performed with this material replacing the extractant phase by acetonitrile (ACN). The results are displayed in Figure 6. The replacement of the water phase by pure ACN resulted in an overall similar removal of DBT from the fuel phase, achieving 77% in 8 h of reaction. Nevertheless, the kinetic profile was much more accelerated in the case of ACN as the extractant, due to the pure extraction effect (ca. 50%–60%) of DBT in the presence of ACN (Figure S6).

Two co-catalysts were also added to the ACN system (H_2SO_4 and FA). Adding either H_2SO_4 or FA to ACN resulted in an increased activity toward the removal of DBT from the fuel phase, leading to ca. 85% of DBT removal in 2 h of reaction. Increasing the reaction time to 8 h resulted in a removal of up to 91%. The addition of FA resulted in a less pronounced H_2O_2 conversion, whereas the addition of H_2SO_4 resulted in accelerated H_2O_2 decomposition when ACN is used as extractant. The increased removal of DBT in the presence of both acids may be linked to the lowering of the medium pH (initial pH of ca. 3.0–3.3), which is associated with a higher yield of oxidizing species, such as hydroxyl radicals,[53] given that the redox potential of both H_2O_2 and $HO^{\bullet}$ is influenced by the pH, with lower pHs significantly increasing their redox potential.[54]

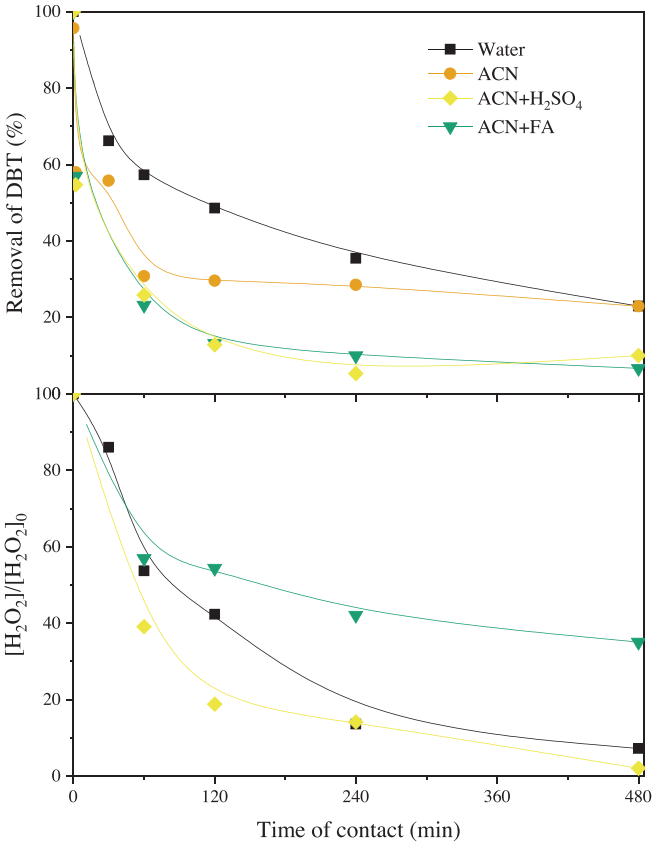

Figure 6. a) Removal of DBT from the oil phase and b) decomposition of H_2O_2 upon time-of-reaction using CNT-POL-OX as a catalyst while varying the extractant and co-catalysts. Conditions: [DBT]0 = 500 mg L^{-1} in 2,2,4-trimethylpentane, O/E volume ratio of 80:20, [catalyst] = 2.5 g L^{-1} (considering the whole volume of the system), T = 70 °C, 0.1 volextractant.% of 1 M H_2SO_4 or FA.

2.2.4. Reaction Products

DBT and its main oxidized products (DBT 5-oxide and DBT 5,5-dioxide) were followed in the extractant phase, and the results are depicted in Figure 7. As seen, when ACN is used as an extractant, DBT is initially extracted. For pure ACN or ACN with H_2SO_4, DBT concentration in the extractant phase reaches its peak within the first 30–60 min of the reaction (Figure 7a) and accumulates in the extractant phase. On the other hand, when using formic acid as a co-catalyst, the maximum concentration of DBT in the extractant phase is only reached at 1 h of reaction, likely because FA resulted in a much faster formation of oxidized intermediates (Figure 7b,c). Using FA as co-catalyst resulted in the highest conversion of DBT into DBT 5-oxide (Figure 7b), peaking at around 2 h of reaction, with ca. 28% of the initially loaded S in the system (equivalent to a concentration of ca. 620 mg L^{-1}). As the reaction moves further, the concentration of DBT 5-oxide decreases to ca. 500 mg L^{-1} (20% of the initially loaded S). The concentration of DBT 5,5-dioxide (Figure 7c), in turn, only achieves its peak by the end of the reaction (ca. 35% of the initially loaded S, ca. 980 mg L^{-1}).

The presence of FA in the can yield performic acid (HCOOOH)[55] upon reaction with H_2O_2. Performic acid has a

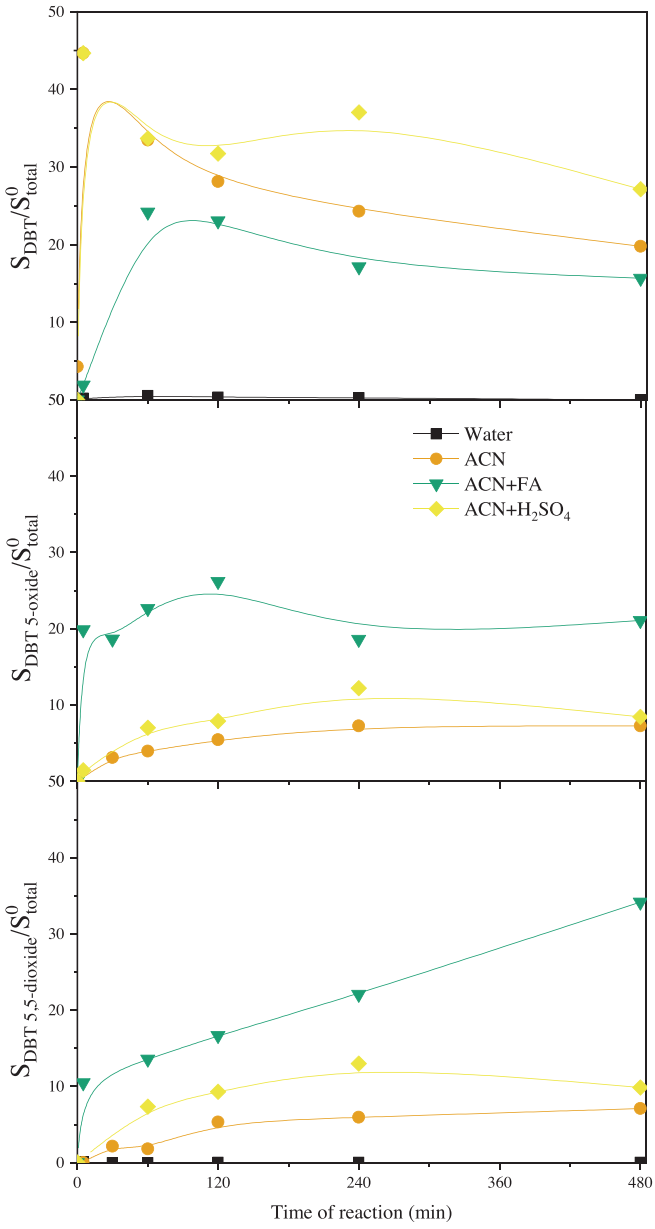

Figure 7. a) DBT in the extractant phase and formation of b) DBT 5-oxide and c) DBT 5,5-dioxide using CNT-POL-OX as catalyst while varying the extractant and co-catalysts. Conditions: [DBT]0 = 500 mg L^{-1} in 2,2,4-trimethylpentane, [H_2O_2]0 = 5.5 g L^{-1} (O/S molar ratio of 15), O/E volume ratio of 80:20, [catalyst] = 2.5 g L^{-1} (considering the whole volume of the system), T = 70 °C, 0.1 volextractant.% of 1 M H_2SO_4 or FA.

higher potential for direct oxygen transfer compared to H_2O_2 due to a more polarized O—O bond.[56] Additionally, H_2O_2 can also yield hydroxyl radicals (redox potential of 2.80 V_{SHE} at acidic pH[57]) in the presence of suitable catalysts (such as CNT-POL-OX), contributing to oxidation through a radical pathway. In the ACN/FA/H_2O_2 system, both pathways are expected to contribute to oxidation, whereas, in the ACN/H_2SO_4/H_2O_2 system, oxidation is expected to be primarily radical-driven due to the absence of performic acid formation. To assess the role of hydroxyl radicals in each system, radical scavenger experiments were performed using ethanol, and the results are depicted in Figure S15. In the ACN/H_2SO_4/H_2O_2 system, ethanol addition reduced the formation of DBT 5-oxide (from 8% to 5%) and DBT 5,5-dioxide (from 10% to 4%) after 8 h, confirming that oxidation predominantly occurs via radical pathways. In contrast, in the ACN/FA/H_2O_2 system, although a decrease in oxidation was also observed, the effect was less pronounced, with DBT 5-oxide formation reducing from 21% to 18%, and DBT 5,5-dioxide from 34% to 20% after 8 h. This suggests that while hydroxyl radicals contribute to oxidation in the FA-containing system, direct oxygen transfer from performic acid also plays a significant role.

To further elucidate the effect of FA, additional experiments were conducted (Figure S16): (i) in the absence of H_2O_2 and (ii) with FA introduced at 60 min. No significant DBT conversion was observed without H_2O_2, confirming that FA alone does not induce oxidation. However, when FA was added after 60 min, DBT 5-oxide formation increased sharply from ~5% to ~20% within 5 min. (data was collected at 65 min to allow for FA homogenization). Simultaneously, DBT concentration in the ACN phase decreased from 35% to 17%, with DBT removal in the oil phase increasing from 61% to 74% within the same timeframe. The effect on DBT 5,5-dioxide formation was minimal. These findings indicate that FA significantly accelerates DBT oxidation upon introduction, reinforcing its role in enhancing oxidation efficiency via performic acid formation.

When water is used as an extractant, it is barely possible to identify DBT or its oxidized intermediates in the water phase, and a significant fraction of the initially loaded S (39%–43%) cannot be identified (Figure S14b). In the Water/H_2SO_4/H_2O_2 system, the radical-induced pathway is expected to be the sole oxidation mechanism. Given the high redox potential of hydroxyl radicals and supporting evidence from the literature related to the over-oxidation of DBT 5,5-dioxide,[58,59] we anticipate that DBT 5,5-dioxide undergoes further oxidation into other molecules. Such conclusion was also drawn upon analyzing the TOC of the aqueous phase (Figure S17) which could not be explained by the theoretical TOC arising from DBT, DBT 5-oxide, or DBT 5,5-dioxide. To investigate which compounds were being formed, oil and extractant phases of selected systems were analyzed by GC-MS. The chromatogram for extractant and oil phases is shown in Figures S18 and S19, respectively. As seen, ACN as extractant results in less DBT in the organic phase compared to water, especially in combination with FA, further confirming the deep desulfurization achieved under this system. Furthermore, it is also possible to identify DBT 5,5-dioxide in the organic phase for reactions carried out with ACN, indicating that oxidation can take place in the oily phase or at the interface between oil-ACN phase. The concentration of DBT 5,5-oxide found in the oil phase corresponds to ca. 5 and 15 mg L^{-1} for ACN/H_2SO_4 and ACN/FA, respectively (equivalent to ca. 0.85% and 2.5% of the initially loaded S).

Other reaction products were observed in the reactions carried out in the presence of water as extractant, such as a reaction product with an m/z of 154 (mass spectra Figure S20), which has been ascribed to biphenyl (95% of correspondence), indicating that the DBT molecule loses the sulfur atom. Previous reports have indicated that C—S cleavage may take place in the presence of H_2O_2[60] and in reactions using water

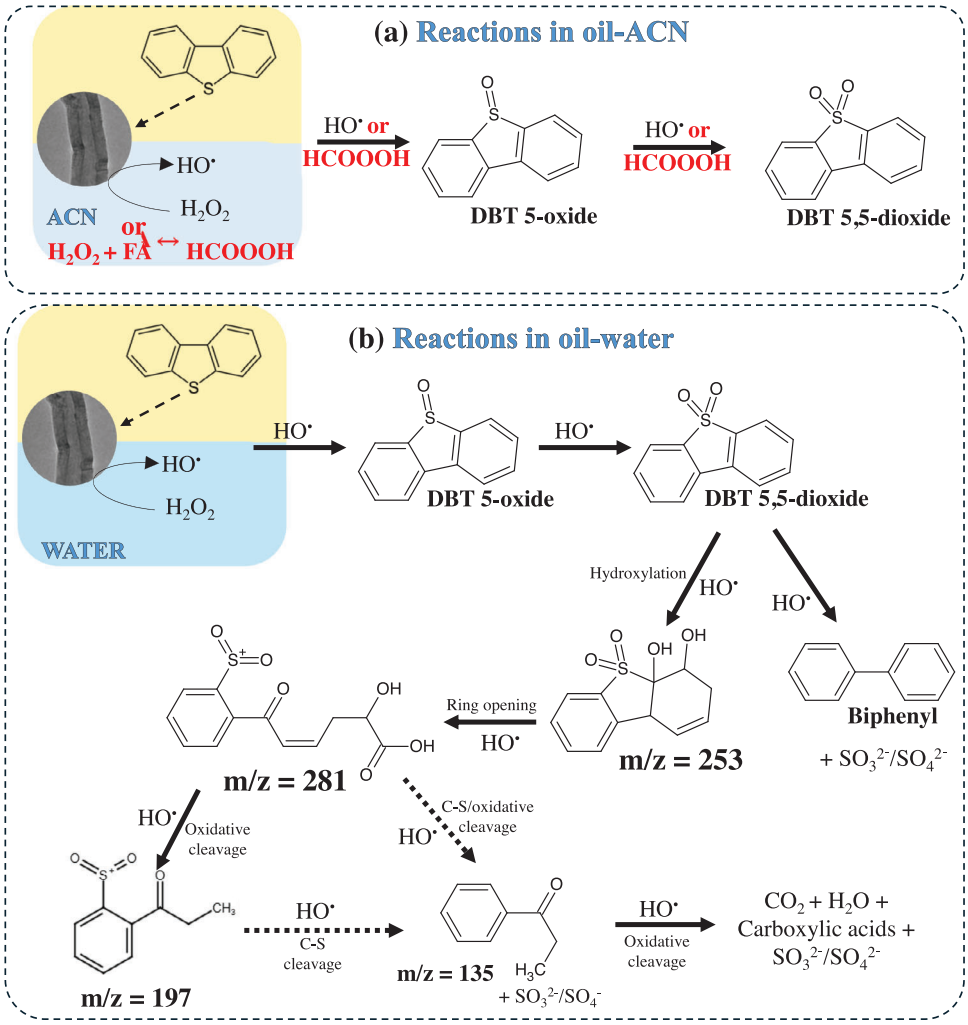

Figure 8. Possible reaction pathway in biphasic systems: a) oil-ACN and b) oil–water.

phases,[61] although such reports are more common for UV-[62–64] or ultrasound-assisted[65,66] desulfurization. Desulfurization processes where C—S cleavage is achieved are highly advantageous, as the removal of bulky sulfonated molecules such as DBT 5,5-dioxide may result in a significant loss of carbon (which means, in fact, a loss of fuel), especially for oily phases with high initial sulfur content.[67] CNT-POL-OX also resulted in other products with m/z of 253, 281, 197, and 135 in the oil phase (Figure S18b) and water phase (Figure S19).

Based on the results gathered, a mechanism for the degradation of DBT in biphasic systems has been proposed (Figure 8). Initially, DBT is adsorbed at the catalyst surface, which should display an adequate water contact angle, graphitization degree, oxygen content, and basic groups (as previously identified as the key reasons for CNT-POL-OX high activity). For reactions carried out in the oil-ACN system, oxidation follows two possible pathways: (i) radical-driven oxidation, where H_2O_2 is decomposed into hydroxyl radicals (HO•) by a suitable catalyst or (ii) direct oxygen transfer (if FA is present), where formic acid reacts with H_2O_2 to generate performic acid (HCOOOH). In the oil-ACN system, only two oxidized products are observed, DBT 5-oxide and DBT 5,5-dioxide (Figure 8a). This is likely due to the lower redox potential of HCOOOH (reported as 1.537 V_{SHE}[68]) and reduced reactivity of hydroxyl radicals in the presence of aprotic solvents, such as ACN,[69] resulting in a more controlled and selective oxidation.

For the water–oil biphasic system, only the radical-driven pathway is expected, as no direct oxygen transfer agent is present. A suitable catalyst facilitates H_2O_2 decomposition into HO• radicals, which oxidize DBT stepwise to DBT 5-oxide and DBT 5,5-dioxide. Given the high redox potential of HO•,[57] C—S bond cleavage occurs, yielding biphenyl, similarly as reported elsewhere,[59] and sulfate species (SO_3^{2-}/SO_4^{2-}), which dissolve into the oily and aqueous phase, respectively. Mass spectrometry (GC-MS) analysis revealed additional oxidation products. A product with m/z 253 is likely a hydroxylated derivative of DBT 5,5-dioxide, formed through additional hydroxyl radical attack. Further oxidation results in ring opening, forming a compound with m/z of 281, which subsequently can cleavage into smaller species of m/z 197 and 135 (which can also result from C—S cleavage from the molecule with m/z 197), similar to what has been reported elsewhere.[65] These byproducts, predominantly found in the aqueous phase, may undergo further oxidation to carboxylic acids, water, and carbon dioxide. The MS spectra of the

possibly oxidized products are shown in Figure S21. Other products were also observed at the chromatograms (retention times of 42.7, 48.8, 50.7, and 60.1 min, Figures S18b and S19) but it was not possible to identify them.

Table S1 reports a series of ODS using carbon-based materials using H_2O_2 as oxidant and either water[11,55,70,71] or acetonitrile[72–74] as extractant phases. Reactions carried out in an oil-acetonitrile biphasic system have been reported using a catalyst concentration in the range 0.8–10 g L^{-1}, an H_2O_2/S molar ratio of 3–330, a temperature of 25–60 °C, for reaction times of 60–120 min, for an initial sulfur concentration of 0.8–2189 ppm, yielding desulfurization from 80% to 100%. For water-oil biphasic systems, reports indicate desulfurization in the range of 20–100% for initial sulfur concentration in the range of 17–1400 ppm, using catalyst concentration in the range 0.5–3.33 g L^{-1}, temperature 25–90 °C, H_2O_2/S molar ratio of 40–1000, and reaction times of 12–120 min. The present work achieved comparable results (77–91%) using significantly less H_2O_2 (H_2O_2/S of 15) and similar catalyst concentration (2.5 g L^{-1}) and temperature (70 °C), although it did require significantly higher reaction times (up to 4 h for ACN as extractant and 8 h for water as extractant).

3. Conclusion

This study effectively synthesized CNTs from plastic solid waste using chemical vapor deposition (CVD) and evaluated their catalytic performance in ODS of fuels. While the polymer source did not significantly affect the yield, it did affect several characteristics of the final product. CNTs from polyolefins (CNT-POL, CNT-POL-P, and CNT-POL-OX) exhibited superior structural integrity, with fewer defects (D/G = 0.64–0.99) compared to CNTs containing PS in the feedstock (D/G = 1.17–1.71). This increased concentration of defects from PS-derived materials affected all other characteristics of the product, including the oxygen content (>9% for PS-containing materials versus <4.4% for the remaining), thermal oxidation (<600 °C for PS-containing materials) and contact angle (50–100° for PS-containing materials versus >117° for POL-derived materials). Furthermore, acid treatment, particularly with nitric acid, allows for enhancing the surface area (>214 m^2 g^{-1}) and reducing the ash content (<5%), also affecting the contact angle of the CNTs (<126° v 138° for CNT-POL).

The distinct characteristics of the materials obtained, given the polymer source or the acid treatment used, also affected the catalytic activity of the materials. CNT-POL-OX achieved the highest desulfurization efficiency, with 77% DBT removal, while CNT-PS-OX reached only 42% under a water-oil biphasic system. Key material's characteristics (such as oxygen content, basicity, suitable wettability, and graphitization degree) were correlated with CNT-POL-OX activity toward DBT removal. The use of co-catalysts and ACN as extractant also impacted the performance, with an ACN-oil biphasic system and formic acid as co-catalyst further increasing DBT removal to 91% using CNT-POL-OX. Despite lower desulfurization, ODS using water as an extractant caused the cleavage of the C-S bond in the bulky DBT molecule, resulting in true desulfurization.

These results demonstrate that CNTs derived from polymers, in particular polyolefins, are promising for deep desulfurization, aligning with both waste valorization and cleaner fuel production goals. By replacing traditional non-renewable carbon sources with plastic waste, this approach helps reduce plastic accumulation in landfills and decreases reliance on fossil resources. Furthermore, it offers a more sustainable and circular pathway for upcycling plastic waste while enhancing fuel purification efficiency, contributing to a greener and more eco-friendly fuel production process.

4. Experimental Section

4.1. Reactants

Hydrochloric acid (37%) and sodium chloride (98%) were provided by VWR Chemicals. Iron (III) chloride tetrahydrate ($FeCl_3{\cdot}6H_2O$, ACS reagent), dibenzothiophene (DBT, 98%), and ammonia solution (28%–30%) were obtained from Merck Chemicals. Sulfuric acid (98%), sodium hydroxide pearls (98%), and formic acid (FA, 98%) were supplied by Labkem. 2,2,4-Trimethylpentane (99.5%), cyclohexane (99.99%), acetonitrile (ACN, 99.9%), propan-2-ol (99.8%), ethanol absolute (99.8%), nickel(II) chloride hexahydrate ($NiCl_2.6H_2O$, analytical reagent grade) and hydrogen peroxide (60% w/v) were provided by Fisher Scientific. Nitric acid (69%) was provided by PanReac AppliChem. Potassium bromide (99%) was obtained from Acros Organics. Spray Mount was provided by 3 M. Aluminum oxide (99.7%) was provided by Thermo Scientific. High-density polyethylene (HDPE; Melt Index 2.2 g/10 min; 190 °C/2.16 kg), low-density polyethylene (LDPE; Average Mw ~35.000 by GPC, Average Mn ~7.700 by GPC), polypropylene (PP; Average Mw ~250.000; Average Mn ~67.000), polystyrene (PS; Average Mw—192000), dibenzothiophene sulfone (DBT 5,5-dioxide, 97%), dibenzothiophene 5-oxide (DBT 5-oxide, 97%), and titanium(IV) oxysulfate solution ($TiOSO_4$, 99.99% trace metal basis) were provided by Sigma-Aldrich Chemistry. n-Hexadecane (99%) was provided by Alfa Aesar. Alumina was provided by BASF (D10-10) in the form of pellets. Prior to use, the pellets were ground and sieved to obtain particles in the size of 53–108 µm.

4.2. Synthesis of Materials

A bimetallic catalyst of nickel ferrite supported over alumina ($NiFe/Al_2O_3$) was synthesized by sol-gel methodology, assuming a 20% deposition of the nickel ferrite over the alumina. The sol-gel procedure was conducted as follows: 10 mmol of M^{2+} ($NiCl_2.6H_2O$) was dissolved in 20 mL of ethanol and heated until reaching its boiling point, and 20 mmol of M^{3+} ($FeCl_3.6H_2O$) was dissolved in 80 mL of ethylene glycol and heated to 60 °C for 5 min. Both solutions were then inserted into an ice bath until reaching temperature equilibrium. The choice of a M^{2+}/M^{3+} molar ratio of 2 was based on previous works related to the sol–gel synthesis of other ferrites.[75] The solutions were mixed in one beaker with Al_2O_3 (6.6 g), and the mixture was heated to 60 °C for 2 h in a heating plate with stirring. Then, the temperature increased to 120 °C, and the mixture was left at this temperature until reaching a gel-like texture (ca. 3 h). Once the gel-like texture was achieved, the temperature increased to 200 °C until a powder texture was reached. The particles were dried in an oven (60 °C, 12 h) and subjected to a calcination process under air atmosphere (850 °C, 3 h), leading to $NiFe/Al_2O_3$.

The catalyst $NiFe/Al_2O_3$ was used to grow CNTs by chemical vapor deposition (CVD), using polymers as carbon sources to

represent typically found polymers in plastic solid waste (PSW). Four polymers were used, namely LDPE, HDPE, PP, and PS, in three different compositions. CNT-POL is derived from a mixture of the three polyolefins (LDPE, HDPE, and PP) at a mass ratio of 35:25:40, CNT-PS is derived from PS, and CNT-MIX from a mixture of the four polymers in a mass proportion of 31:23:35:11 (LDPE:HDPE:PP:PS). The mass proportions used were chosen to simulate typical compositions of PSW, as reported elsewhere.[76] The CVD process was carried out in a single-stage pyrolysis oven (TH/TV, Termolab),[18] considering 1 g of CVD catalyst per 5 g of polymer or polymer mixture. The CVD reactions were conducted at 850 °C for 1 h under a nitrogen flow of 50 mL min^{-1}. By the end of the reaction, the reactor was allowed to cool down to room temperature under the same nitrogen flow. The yield of CNTs was determined according to Equation 1.

$$Yield\ (\%) = \frac{carbon\ in\ the\ CNTs}{carbon\ in\ the\ polymer} X\,100 \quad (1)$$

After the synthesis, CNT-POL was subjected to an acid wash (50 wt.% H_2SO_4, 140 °C, 3 h) to remove metal particles, leading to CNT-POL-P. CNT-POL, CNT-PS, and CNT-MIX were subjected to a stronger oxidation with nitric acid (69 wt.% HNO_3, 130 °C, 24 h) to introduce oxygenated moieties, which have been correlated with higher ODS activity,[2] leading to CNT-POL-OX, CNT-PS-OX, and CNT-MIX-OX, respectively. All materials were carefully washed with distilled water after acid treatment until the rising water reached neutrality.

4.3. Materials Characterization

The materials were characterized by FT-IR (PerkinElmer spectrophotometer) using KBr pellets from 450 to 4000 cm^{-1} with a resolution of 4 cm^{-1}. The textural properties of the materials were determined using a NOVA TOUCH LX4 equipment from Quantachrome Instruments, as reported elsewhere.[21] The Ni and Fe content of the particles was determined upon digestion of the ashes of the samples with aqua regia (105 °C, 12 h). The resulting liquid was filtered (pore: 0.45 µm) and the liquid was analyzed by atomic absorption (SpectrAA, Varian). Static contact angles were obtained by the sessile drop method. The samples were prepared by covering a glass slide with the aid of a spay adhesive from 3 M, as reported elsewhere.[77] Any loose particles were gently removed, and the prepared glass slides were dried overnight (80 °C). At least three distinct measurements were performed per sample with the aid of an Attension optical tensiometer (model theta) and the images recorded were processed using ImageJ. The basicity and acidity of the samples were determined as reported in previous studies.[78] CNHS—O content was obtained in a Flash 2000 analyzer (Thermo Fisher Scientific, Waltham, MA, USA) provided with a thermal conductivity detector (TCD). TGA analysis was performed in a NETZSCH TG 209F3 in air atmosphere from 30 to 930 °C at a rate of 10 °C min^{-1}. Raman spectra were acquired in an Alpha 300 equipment (WiTec, Germany) at a 532 nm monochromatic wavelength. The data were processed (removal of cosmic ray, baseline removal and normalization) using Project Five v5.3. Deconvolution of Raman peaks was carried out with Origin software, and the D/G ratio was calculated based on the deconvoluted area. XRD analyses were made at room temperature using a PANalytical X'Pert Pro diffractometer equipped with an X'Celerator detector and secondary monochromator in $\theta/2\theta$ Bragg-Brentano geometry. The measurements were carried out using 40 kV and 30 mA, a CuKa radiation ($\lambda_{\alpha1}$ = 1.54060 Å and $\lambda_{\alpha2}$ = 1.54443 Å), 0.017°/ step, 100 s/step, in a 10–80° 2θ angular range. The results obtained were processed in the software HighScore Plus. TEM images were obtained using a JEOL 1011 transmission electron microscope operating at 200 kV. The diameter of CNTs was estimated using ImageJ.

4.4. Oxidative Desulfurization

The ODS reaction was carried out at 70 °C for 8 h of reaction. Initially, water with H_2SO_4 (0.1 vol_{water}% of a 1 M solution, resulting in a pH of 3.0) was used as the extractant phase. The DBT solution in 2,2,4-trimethylpentane ($[DBT]_0$ = 500 mg L^{-1}) was heated to 70 °C, and then the extractant was added to reach an oil-to-extractant (O/E) volume ratio of 80:20. Both phases were thoroughly mixed (600 rpm) for 5 min. Hydrogen peroxide ($[H_2O_2]_0$ = 5.5 g L^{-1}, O/S = 15) was added, followed by catalyst ([catalyst] = 2.5 g L^{-1}, considering the whole volume of the system), marking this instant as t = 0 min. The reaction was periodically monitored by removing liquid samples (respecting the O/W volume ratio). DBT concentration and intermediates were followed in the oily and aqueous phases by GC-FID and HPLC, respectively, and H_2O_2 was followed by UV–vis. By the end of the reaction, the catalyst was separated from the reaction medium by filtration, and each phase was stored separately. The adsorbed compounds in the catalyst phase were extracted by sonication with acetone (30 min, [cat] = 1 mg mL^{-1}, room temperature). The liquid was then filtered and analyzed by HPLC. A non-catalytic run was carried out in the absence of catalyst.

The extractant phase was replaced by (i) pure acetonitrile, (ii) acetonitrile modified with H_2SO_4 (0.1 vol_{water}% of a 1 M solution), and (iii) acetonitrile modified with formic acid (0.1 vol_{water}% of a 1 M solution). The reaction procedure was followed as described above.

The effect of formic acid in the abovementioned system was further evaluated by a reaction carried out in the presence of CNT-POL-OX and in the absence of hydrogen peroxide (following every other condition as already mentioned), and by delayed addition of formic acid to the ACN/FA/H_2O_2 system (FA added at 60 min of reaction; all remaining experimental conditions maintained the same). The role of hydroxyl radicals was assessed by adding ethanol (molar ratio H_2O_2:EtOH of 2) to the ACN/FA/H_2O_2 and ACN/H_2SO_4/H_2O_2 systems.

The efficiency of the use of hydrogen peroxide ($n_{H_2O_2,t}$) at time t during ODS reactions was estimated by Equation 2.

$$n_{H_2O_2,t} = \frac{X^{oil}_{DBT,t}}{X_{H_2O_2,t}} \quad (2)$$

In which $X^{oil}_{DBT,t}$ is the removal of DBT from the oil phase and $X_{H_2O_2,t}$ is the conversion of hydrogen peroxide at time t (both dimensionless).

The adsorption ability of the materials toward DBT ($[DBT]_0$ = 500 mg L^{-1} in 2,2,4-trimethylpentane) was also considered. A volume of the DBT solution was placed in a reaction vessel and heated to 70 °C. Upon reaching the desired temperature, the adsorbent was added ([adsorbent] = 2.5 g L^{-1}), considering this time t = 0 min. The adsorption was allowed to proceed for 8 h. DBT was measured using UV–vis.

Extraction runs were conducted by placing the oily phase in contact with distinct extractant phases (water, acetonitrile (ACN), acetonitrile and FA, and acetonitrile and H_2SO_4) and samples were withdrawn to measure the concentration of DBT in each phase by UV–vis.

4.5. Analytical Methods

Hydrogen peroxide was measured by complexation with $TiOSO_4$ and reading the solution by UV–vis at 405 nm, as described in

previous work.[78] DBT was followed by UV–vis at 235 nm for adsorption and extraction runs, both for oily and water phases. For ODS runs, DBT in the oily phase was followed by gas chromatography coupled to flame ionization detection (GC-FID Varian 3800) using n-hexadecane as the internal standard (1 mg mL^{-1}). The operating conditions used for GC analysis were a helium flow (carrier gas) of 1 mL min^{-1} and an initial oven temperature of 50 °C, which was held for 5 min. Then, a ramp was performed up to 270 °C at 15 °C min^{-1} rate, which was held for 2 min, leading to a total running time of 20 min. The injection temperature was 250 °C, and the detector temperature was 200 °C, and all the analysis was made with a split ratio of 20. DBT and its oxidized intermediates in the extractant phases were followed by High Pressure Liquid Chromatography (JASCO System). The separation of the reaction products was achieved in a Restek Ultra Biphenyl column (15 cm x 2.1 mm, particle size 5 µm) and an isocratic mobile phase (50% acetonitrile and 50% ultrapure water with orthophosphoric acid (0.1 vol.%)) with a 0.3 mL min^{-1} flow delivered by a quaternary pump (PU-2089). The detection was achieved in a UV–vis spectrophotometer at 235 nm (UV-2075). The reaction products in the extractant phase and oily phase were further confirmed by gas chromatography coupled with mass spectroscopy (GCMS-QP2020, Shimadzu). Prior to analysis, for the water phase, 100 µL of the water phase was mixed with 2 mL of 2,2,4-trimethylpentane and mixed with the aid of an ultrasound bath. Then, the water was dried with excess sodium sulfate and the supernatant was collected and filtered (pore: 0.22 µm). Oil phases were simply filtered. The operating conditions for the oven were a helium flow (carrier gas) of 1 mL min^{-1} and an initial oven temperature of 50 °C (held for 3.5 min), followed by a ramp up to 300 °C at 3 °C min^{-1} rate (held for 15 min), leading to a total running time of 101 min, using a split ratio of 20. The injection temperature was 250 °C. N-hexadecane was used as an internal standard (1 mg mL^{-1}). TOC of the aqueous phase of the reaction carried out with CNT-POL-OX was measured using Shimadzu equipment (TOC L CSH/CSN).

Supporting Information

The supporting information contains the following items: Figure S1. XRD and FTIR of CVD catalyst; Figure S2. COD cards for identification of XRD data; Figure S3. Yield of CNTs and mass loss during acid washing; Figure S4. CNT's outer diameters distribution; Figure S5. Correlation between the percentual of PS in the feedstock and D/G ratio of the materials; Figure S6. N_2 adsorption-desorption isotherms; Figure S7. Correlation between material's characteristics; Figure S8. Pure extraction effect in ODS reactions for POL-derived CNTs; Figure S9. Correlation between ODS results and materials' characteristics; Figure S10. DBT adsorption and correlation with oxygen content; Figure S11. DBT and others desorbed from the catalyst after ODS; Figure S12. Efficiency on hydrogen peroxide use; Figure S13. Correlation between ODS results and materials characteristics for oxidized CNT samples; Figure S14. ODS with ACN + FA in the absence of hydrogen peroxide and delayed FA addition; Figure S15. ODS with the addition of a radical scavenger; Figure S16. Distribution of S at the end of ODS; Figure S17. TOC; Figure S18. GC-MS chromatogram for oil phase; Figure S19. GC-MS chromatogram for water phase; Figure S20. Mass spectra of biphenyl; Figure S21. Mass spectra of other oxidized intermediates. Table S1. Reported ODS reactions.

Acknowledgements

This work was financially supported by national funds through FCT/MCTES (PIDDAC): CIMO, UIDB/00690/2020 (DOI: 10.54499/UIDB/00690/2020) and UIDP/00690/2020 (DOI: 10.54499/UIDP/00690/2020); SusTEC, LA/P/0007/2020 (DOI: 10.54499/LA/P/0007/2020); LSRE-LCM, UIDB/50020/2020 (DOI: 10.54499/UIDB/50020/2020) and UIDP/50020/2020 (DOI: 10.54499/UIDP/50020/2020); ALiCE, LA/P/0045/2020 (DOI: 10.54499/LA/P/0045/2020). F.F.R. acknowledges the national funding by FCT and the European Social Fund, FSE, through the individual research grant SFRH/BD/143224/2019. A.S.S. was supported by the doctoral grant SFRH/BD/151346/2021, financed by FCT with funds from NORTE2020, under MIT Portugal Program. J.L.D.T. acknowledges the financial support through the program of Atracción al Talento of Comunidad de Madrid (Spain) for the individual research grant 2022-T1/AMB-23946. The authors are also grateful for the finantial support provided by Sociedade Ponto Verde for the project "*Estudo técnico-económico para a valorização de resíduos de embalagens plásticas na produção de nanotubos de carbono*".

Conflict of Interests

The authors declare no conflict of interest.

Data Availability Statement

The data that support the findings of this study are available from the corresponding author upon reasonable request.

Keywords: Chemical vapor deposition · Fenton-like · Nanomaterials · Oxidative desulfurization · Waste valorization

[1] J. Davenport, N. Wayth, *Energy Institute* **2024**, 1–76.
[2] F. F. Roman, J. L. Diaz de Tuesta, A. M. T. Silva, J. L. Faria, H. T. Gomes, *Catalysts* **2021**, *11*, 1239.
[3] Y. Wu, R. Li, L. Cui, Y. Meng, H. Cheng, H. Fu, *Chemosphere* **2020**, *241*, 125031.
[4] A. Haruna, Z. Merican Aljunid Merican, S. Gani Musa, S. Abubakar, *Fuel* **2022**, *329*, 125370.
[5] M. Hossain, H. Park, H. Choi, *Catalysts* **2019**, *9*, 229.
[6] F. S. Mjalli, O. U. Ahmed, T. Al-Wahaibi, Y. Al-Wahaibi, I. M. AlNashef, *Rev. Chem. Eng.* **2014**, *30*, 337–378.
[7] M. Adhami, S. Movahedirad, M. A. Sobati, *J. Sulfur Chem.* **2022**, *43*, 685–712.
[8] A. Guntida, D. S. S. Jorqueira, C. Nikitine, P. Fongarland, K. Thomas, F. Maugé, J. Aparicio, *Biomass Bioenergy* **2024**, *188*, 107341.
[9] I. Shafiq, S. Shafique, P. Akhter, M. Ishaq, W. Yang, M. Hussain, *J. Cleaner Prod.* **2021**, *294*, 125731.
[10] A. Haruna, Z. M. A. Merican, S. G. Musa, *J. Industr. Eng. Chem.* **2022**, *112*, 20–36.
[11] R. V. Mambrini, C. Z. Maia, J. D. Ardisson, P. P. de Souza, F. C. C. Moura, *New J. Chem.* **2017**, *41*, 142–150.
[12] A. Rajendran, T.-y. Cui, H.-x. Fan, Z.-f. Yang, J. Feng, W.-y. Li, *J. Mater. Chem. A* **2020**, *8*, 2246–2285.
[13] S. Zhang, X. He, Y. Ding, Z. Shi, B. Wu, *Renewable Sustainable Energy Rev.* **2024**, *204*, 114821.
[14] N. V. Reutova, T. V. Reutova, F. R. Dreeva, A. A. Shevchenko, *Environ. Geochem. Health* **2022**, *44*, 4557–4568.

[15] F. F. Roman, L. De Grande Piccinin, A. Santos Silva, J. L. Diaz de Tuesta, I. V. K. Freitas, A. Vieira, G. Gonçalves Lenzi, A. M. T. Silva, J. L. Faria, H. T. Gomes, *Catalysts* **2023**, *13*, 1259.
[16] A. Ahamed, A. Veksha, K. Yin, P. Weerachanchai, A. Giannis, G. Lisak, *J. Hazard. Mater.* **2020**, *390*, 121449.
[17] H. Kim, E. Nam, K. An, H. Lim, *Chem. Eng. J.* **2024**, *495*, 153300.
[18] J. L. Diaz de Tuesta, A. S. Silva, F. F. Roman, L. F. Sanches, F. A. da Silva, A. I. Pereira, A. M. T. Silva, J. L. Faria, H. T. Gomes, *Catal. Today* **2023**, *419*, 114162.
[19] R. Zhu, Y. Zhu, H. Xian, L. Yan, H. Fu, G. Zhu, Y. Xi, J. Zhu, H. He, *Appl. Catal., B* **2020**, *270*, 118891.
[20] J. L. Diaz de Tuesta, B. F. Machado, P. Serp, A. M. T. Silva, J. L. Faria, H. T. Gomes, *Catal. Today* **2020**, *356*, 205–215.
[21] F. F. Roman, J. L. Diaz de Tuesta, F. K. K. Sanches, A. S. Silva, P. Marin, B. F. Machado, P. Serp, M. Pedrosa, A. M. T. Silva, J. L. Faria, H. T. Gomes, *Catal. Today* **2023**, *420*, 114001.
[22] K. Hartonen, M.-L. Riekkola, in *The Application of Green Solvents in Separation Processes* (Eds: F. Pena-Pereira, M. Tobiszewski), Elsevier, Amsterdam, **2017**, pp. 19–55.
[23] F. Zhou, Z. Hearne, C.-J. Li, *Curr. Opin. Green Sustain. Chem.* **2019**, *18*, 118–123.
[24] X. Gao, J. Fei, Y. Shang, F. Fu, *Chin. J. Chem. Eng.* **2018**, *26*, 1508–1512.
[25] S. O. Ribeiro, L. S. Nogueira, S. Gago, P. L. Almeida, M. C. Corvo, B. d. Castro, C. M. Granadeiro, S. S. Balula, *Appl. Catal., A* **2017**, *542*, 359–367.
[26] Z. T. Khodair, N. M. Ibrahim, T. J. Kadhim, A. M. Mohammad, *Chem. Phys. Lett.* **2022**, *797*, 139564.
[27] S. Sagadevan, Z. Z. Chowdhury, R. F. Rafique, *Mater. Res.* **2018**, *21*, e20160533.
[28] S. Kazemifard, H. Nayebzadeh, N. Saghatoleslami, E. Safakish, *Environ. Sci. Pollut. Res. Int.* **2018**, *25*, 32811–32821.
[29] A. S. S. Nila, *Int. J. Res. Appl. Sci. Eng. Technol.* **2018**, *6*, 2493–2496.
[30] K. Djebaili, Z. Mekhalif, A. Boumaza, A. Djelloul, *J. Spectrosc.* **2015**, *2015*, 1–16.
[31] K. Li, H. Zhang, Y. Zheng, G. Yuan, Q. Jia, S. Zhang, *Nanomaterials* **2020**, *10*, 1517.
[32] K. A. Graves, L. J. R. Higgins, M. A. Nahil, B. Mishra, P. T. Williams, *J. Anal. Appl. Pyrolysis* **2022**, *161*, 105396.
[33] A. A. Aboul-Enein, A. E. Awadallah, A. A. H. Abdel-Rahman, A. M. Haggar, *Fuller. Nanotub. Carbon Nanostruct.* **2018**, *26*, 443–450.
[34] A. Veksha, W. Chen, L. Liang, G. Lisak, *J. Hazard. Mater.* **2022**, *435*, 128949.
[35] A. Veksha, M. Z. Bin Mohamed Amrad, W. Q. Chen, D. K. Binte Mohamed, S. B. Tiwari, T. T. Lim, G. Lisak, *Chemosphere* **2022**, *297*, 134148.
[36] A. Orbaek White, A. Hedayati, T. Yick, V. S. Gangoli, Y. Niu, S. Lethbridge, I. Tsampanakis, G. Swan, L. Pointeaux, A. Crane, R. Charles, J. Sallah-Conteh, A. O. Anderson, M. L. Davies, S. J. Corr, R. E. Palmer, *Nanomaterials* **2021**, *12*, 9.
[37] L. M. Malard, M. A. Pimenta, G. Dresselhaus, M. S. Dresselhaus, *Phys. Rep.* **2009**, *473*, 51–87.
[38] H. Nakajima, K. Kobashi, Y. Zhou, M. Zhang, T. Okazaki, *Carbon* **2024**, *216*, 18495.
[39] Y.-L. Kuo, W.-M. Hsu, P.-C. Chiu, Y.-H. Tseng, Y. Ku, *Ceram. Int.* **2013**, *39*, 5459–5465.
[40] A. A. S. Oliveira, I. F. Teixeira, T. Christofani, J. C. Tristão, I. R. Guimarães, F. C. C. Moura, *Appl. Catal. B-Environ* **2014**, *144*, 144–151.
[41] L. F. Greenlee, S. A. Hooker, *Desalin. Water Treatm.* **2012**, *37*, 114–121.
[42] L. Zhou, A. Rai, N. Piekiel, X. Ma, M. R. Zachariah, *J. Phys. Chem. C* **2008**, *112*, 16209–16218.
[43] H. U. Modekwe, M. A. Mamo, K. Moothi, M. O. Daramola, *Catalysts* **2021**, 11.
[44] H. Li, N. Zhao, C. He, C. Shi, X. Du, J. Li, *Mater. Sci. Eng, A* **2008**, *473*, 355–359.
[45] M. E. Birch, T. A. Ruda-Eberenz, M. Chai, R. Andrews, R. L. Hatfield, *Ann. Occup. Hyg.* **2013**, *57*, 1148–1166.
[46] S. Morales-Torres, T. L. Silva, L. M. Pastrana-Martinez, A. T. Brandao, J. L. Figueiredo, A. M. Silva, *Phys. Chem. Chem. Phys.* **2014**, *16*, 12237–12250.
[47] C. Qiu, L. Jiang, Y. Gao, L. Sheng, *Mater. Des.* **2023**, *230*, 111952.
[48] F. Wan, D.-Q. Yang, E. Sacher, *J. Mater. Chem. A* **2015**, *3*, 16953–16960.
[49] Z. C. Kampouraki, D. A. Giannakoudakis, K. S. Triantafyllidis, E. A. Deliyanni, *Green Chem.* **2019**, *21*, 6685–6698.
[50] Q. Gu, Y. Ding, Z. Liu, Y. Lin, R. Schlögl, S. Heumann, D. Su, *J. Energy Chem.* **2019**, *32*, 131–137.
[51] S. Dou, Y. Feng, K. Liu, X. Wang, B. Zhang, C. Yang, M. Sun, Y. Liu, F. Cheng, W. Zhou, E. Duan, *Sep. Purif. Technol.* **2024**, *334*, 125992.
[52] H. Liu, C. Liu, N. Zhen, J. Dong, Y. Chi, C. Hu, *Appl. Catal., A* **2023**, *656*, 119133.
[53] A. Fischbacher, C. von Sonntag, T. C. Schmidt, *Chemosphere* **2017**, *182*, 738–744.
[54] G. Yu, S. Lu, H. Chen, Z. Zhu, *Energy Fuels* **2004**, *19*, 447–452.
[55] M. T. Timko, E. Schmois, P. Patwardhan, Y. Kida, C. A. Class, W. H. Green, R. K. Nelson, C. M. Reddy, *Energy Fuels* **2014**, *28*, 2977–2983.
[56] C. Shi, C. Li, Y. Wang, J. Guo, S. Barry, Y. Zhang, N. Marmier, *Water* **2022**, *14*, 2309.
[57] R. S. Ribeiro, A. M. T. Silva, J. L. Figueiredo, J. L. Faria, H. T. Gomes, *Appl. Catal., B* **2016**, *187*, 428–460.
[58] S. A. Hosseini, V. Majidi, A. R. Abbasian, *J. Sulfur Chem.* **2018**, *39*, 119–129.
[59] M. Zarrabi, M. H. Entezari, E. K. Goharshadi, *RSC Adv.* **2015**, *5*, 34652–34662.
[60] N. d'Alessandro, L. Tonucci, M. Bonetti, M. Di Deo, M. Bressan, A. Morvillo, *New J. Chem.* **2003**, *27*, 989–993.
[61] B. Bertleff, J. Claußnitzer, W. Korth, P. Wasserscheid, A. Jess, J. Albert, *ACS Sustainable Chem. Eng.* **2017**, *5*, 4110–4118.
[62] W. Shi, X. Zhou, Y. Kong, J. Li, I. E. Marko, *Chem. Asian J.* **2020**, *15*, 511–517.
[63] S. Moradi, M. Vossoughi, M. Feilizadeh, S. M. E. Zakeri, M. M. Mohammadi, D. Rashtchian, A. Y. Booshehri, *Res. Chem. Intermed.* **2014**, *41*, 4151–4167.
[64] M. Bagheri, M. Y. Masoomi, A. Morsali, *ACS Catal.* **2017**, *7*, 6949–6956.
[65] D. Margeta, I. Grcic, S. Papic, K. Sertic-Bionda, L. Foglar, *Environ. Technol.* **2016**, *37*, 293–299.
[66] I. Grčić, S. Papić, *Appl. Acoust.* **2016**, *103*, 232–238.
[67] G. H. C. Prado, Y. Rao, A. de Klerk, *Energy Fuels* **2017**, *31*, 14–36.
[68] C. Nabintu Kajoka, J. Gasperi, S. Brosillon, E. Caupos, E. Mebold, M. Oliveira, V. Rocher, G. Chebbo, J. L.e Roux, *ACS ES&T Water* **2023**, *3*, 3121–3131.
[69] S. Mitroka, S. Zimmeck, D. Troya, J. M. Tanko, *J. Am. Chem. Soc.* **2010**, *132*, 2907–2913.
[70] J. Xiao, L. Wu, Y. Wu, B. Liu, L. Dai, Z. Li, Q. Xia, H. Xi, *Appl. Energy* **2014**, *113*, 78–85.
[71] I. F. Teixeira, A. A. d. S. Oliveira, T. Christofani, F. C. C. Moura, *J. Mater. Chem. A* **2013**, *1*, 10203–10208.
[72] G. Zhang, F. Yang, W. Yang, Y. Li, *Particuology* **2023**, *81*, 109–118.
[73] N. T. do Prado, A. P. Heitmann, H. S. Mansur, A. A. Mansur, L. C. A. Oliveira, C. S. de Castro, *J. Environ. Sci.* **2017**, *57*, 312–320.
[74] C. Wang, A. Li, J. Xu, J. Wen, H. Zhang, L. Zhang, *J. Chem. Technol. Biotechnol.* **2019**, *94*, 3403–3412.
[75] A. S. Silva, F. F. Roman, A. V. Dias, J. L. Diaz de Tuesta, A. Narcizo, A. P. F. da Silva, I. Çaha, F. L. Deepak, M. Bañobre-López, A. M. C. Ferrari, H. T. Gomes, *J. Environ. Chem. Eng.* **2023**, *11*, 110806.
[76] PlasticsEurope, **2020**, https://plasticseurope.org/knowledge-hub/plastics-the-facts-2020 Accessed: December 15th, 2024.
[77] E. Nowak, G. Combes, E. H. Stitt, A. W. Pacek, *Powder Technol.* **2013**, *233*, 52–64.
[78] A. S. Silva, M. Seitovna Kalmakhanova, B. Kabykenovna Massalimova, J. G. Sgorlon, D. d. T. Jose Luis, H. T. Gomes, *Catalysts* **2019**, *9*, 705.

Manuscript received: February 12, 2025
Revised manuscript received: March 27, 2025
Accepted manuscript online: April 2, 2025
Version of record online: ■■, ■■